CHALMERS
UNIVERSITY OF TECHNOLOGY

Understanding the NH<inf>3</inf> adsorption mechanism on a vanadium-based SCR catalyst: A data-driven modeling approach

Chemical Engineering Science 262 (2022) 117975

Contents lists available at ScienceDirect

Chemical Engineering Science

journal homepage: www.elsevier.com/locate/ces

Understanding the NH_3 adsorption mechanism on a vanadium-based SCR catalyst: A data-driven modeling approach

Andres F. Suarez-Corredor [a,b], Matthäus U. Bäbler [c], Louise Olsson [a], Magnus Skoglundh [a], Björn Westerberg [b]

[a] Competence Centre for Catalysis, Chalmers University of Technology, Gothenburg 412 96, Sweden
[b] Scania CV AB, Södertälje 151 87, Sweden
[c] Department of Chemical Engineering, KTH Royal Institute of Technology, Stockholm 100 44, Sweden

HIGHLIGHTS

- A data-driven modeling framework was developed for ammonia adsorption over a vanadium-based SCR catalyst.
- The proposed model, based on the Langmuir adsorption framework, involves 5 adsorption sites.
- Model parameters, such as the enthalpy and entropy of adsorption, have physical significance comparable with other studies.
- The data-driven modeling framework maximizes the utilization of information from experiments.
- Besides the model parameters, the adsorption model structure is considered as a variable which can be optimized.

GRAPHICAL ABSTRACT

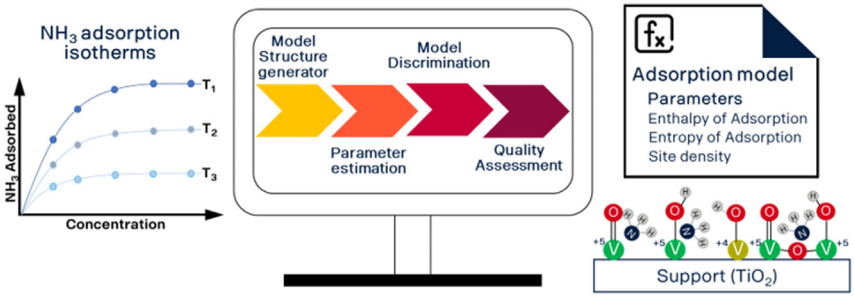

ARTICLE INFO

Article history:
Received 24 March 2022
Received in revised form 23 June 2022
Accepted 1 August 2022
Available online 5 August 2022

Keywords:
Ammonia adsorption
Vanadium-SCR
Parameter estimation
Kinetic studies

ABSTRACT

Ammonia adsorption is a precondition for the selective catalytic reduction (SCR) of nitrogen oxides (NO_x) to take place and it influences catalyst performance under transient conditions. For a vanadium-based SCR catalyst NH_3 adsorption takes place on multiple adsorption sites over the catalyst surface with different behaviours depending on temperature, gas concentration and catalyst oxidation state. In this study, a mechanistic NH_3 adsorption model within the framework of Langmuir adsorption models was developed for describing the NH_3 adsorption isotherms obtained with a gas flow reactor for a vanadium-based SCR. The model was created by a data-driven modeling process, which involves different steps. First, a large set of candidate models was created systematically by combining multiple feasible adsorption mechanisms. Then, a parameter estimation workflow was performed using three different objective functions with increased complexity. Finally, a model reconciliation step was executed and a quality assessment was done for creating a unified robust model with a high degree of validity. As a result of this method, an NH_3 adsorption model with five adsorption sites with different mechanisms was obtained that captures the main features from the experimental data. Furthermore, the model parameters have physical significance and relate to the adsorption strength and spatial arrangement for NH_3 and water molecules. The proposed model can be used in the development of transient models with increased validity over a wide experimental region.

E-mail address: andres.suarez@scania.com (A.F. Suarez-Corredor)

https://doi.org/10.1016/j.ces.2022.117975
0009-2509/

1. Introduction

Sustainable transportation involves several road-maps where multiple technologies are developed and improved towards the reduction of the impact on the planetary boundaries of our ecosystem (Gross, 2020; Teter et al., 2017). Technologies are aimed to mitigate or remediate the impact from our anthropogenic activity (Frey, 2018; Senecal and Leach, 2019). In that aim, the exhaust after-treatment system used for internal combustion engine vehicles reduces the air pollution by converting harmful pollutants, such as NO_x, by using multiple catalysts integrated with a sophisticated control system (Nova and Tronconi, 2014; Heck et al., 2016).

The selective catalytic reduction (SCR) catalyst plays an important role in the emission after-treatment system by reducing NO_x to N_2 in an oxidative environment. The SCR catalyst achieves this through the use of NH_3 which is supplied by an aqueous urea solution (Nova and Tronconi, 2014; Tronconi et al., 2005). Currently, there are two main SCR technologies used in automotive applications: vanadium-based or copper-functionalized zeolite monolith catalysts. The vanadium-based SCR catalyst offers high NO_x conversion in the temperature range from 300 to 450°C, and is robust to chemical poisons such as sulfur and some alkali-metals (Nova and Tronconi, 2014; Wachs and Weckhuysen, 1997). On the other hand the vanadium-based SCR catalyst has lower NH_3 storage capacity and it is more sensitive to high temperatures compared to the copper-functionalized zeolites (Nova et al., 2006; Wachs and Weckhuysen, 1997). Nevertheless, the vanadium-base SCR catalyst offers adequate performance, with high selectivity and prolonged durability if the temperature is controlled to avoid vanadium sublimation and the urea dosing is calibrated properly. In fact, vanadium-based SCR catalysts are essential for future emission after-treatment systems as they complement other technologies such as copper-functionalized zeolites, making the system more robust and with a wider operating region.

New legislation on fuel efficiency and reduction of CO_2 emissions could lead to an increase of engine-out NO_x emissions which will increase the demand on the SCR catalyst. Dealing with this scenario will require better understanding of the SCR catalysts, its main features and reaction mechanisms (Tronconi et al., 2005; Teter et al., 2017). The best strategy for establish understanding is by the development of models that are able to capture the main features and phenomena involved in a process. The importance of an SCR catalyst model is evident in the emission after-treatment system proposal for the future CARB emission legislation in California, where a model-based strategy for NH_3 storage control is suggested (Sharp et al., 2021; Zavala et al., 2020). The idea is that the control strategy keeps track on the NH_3 storage capacity and the NH_3 distribution among the different SCR catalysts in the system by using NO_x and NH_3 sensors (Zavala et al., 2020).

NH_3 adsorption is one of the main reaction steps for the SCR catalyst since it is a prerequisite for the SCR reaction to occur. In the SCR mechanism, NH_3 activates the adsorption site to react with NO_x which is assumed to not be adsorbed or weakly adsorbed over the catalyst surface (Tronconi et al., 2005; Topsøe, 1994). Moreover, NH_3 adsorption relates to the NH_3 storage capacity of the catalyst which affects the transient behavior and the urea dosing strategy in the emission after-treatment system. An accurate estimation of the NH_3 adsorption phenomena enables further optimization of the current system to fulfill future stricter emission legislation, reducing NH_3 slip, minimizing side reactions and improving the urea dosing control (Lietti et al., 1997; Nova and Tronconi, 2014).

In a vanadium-based SCR catalyst, formulating a detailed intrinsic mechanism is a challenge due to the diversity of species over the catalyst, where vanadium forms different structures with different behavior and interactions with the support (TiO_2) and promoters such as tungsten (W). Topsøe et al. proposed a reaction cycle for a vanadium-based SCR catalyst composed of both acid and redox reactions (Topsøe, 1994). In this mechanism, NH_3 is adsorbed on an acid Brønsted site, and reacts with NO to produce N_2 and water, thereby reducing the vanadium site which then is regenerated by O_2 in the redox cycle. Arnarsson et al. complemented the previous mechanism by including the standard and fast SCR reactions in a combined cycle (Arnarson et al., 2017). Moreover, Lian et al. defined different cycles for monomeric and polymeric vanadium sites, explaining the high activity of the polymeric form compared to the monomeric one (He et al., 2018).

There are multiple sites for NH_3 adsorption in a vanadium-based SCR catalyst. These sites can be active sites for the SCR reaction or they can serve as NH_3 reservoirs, not involved in the SCR reaction. The active sites can be referred to different vanadium species over the catalyst, while the NH_3 reservoirs are the catalyst support and promoters (Wachs and Weckhuysen, 1997; Tronconi et al., 2005; Nova et al., 2006). First principles studies, including density functional theory (DFT) calculations, suggest that NH_3 can be adsorbed on a vanadium atom in different configurations with different bonding energies(Anstrom et al., 2002; Vittadini et al., 2005). For instance, NH_3 can adsorb on a monomeric vanadium species on the V-OH adjacent to the support, which is more feasible if the monomeric vanadium is adjacent to one promoter atom (W) (Anstrom et al., 2003; Yin et al., 1999). For the polymeric vanadium, there are different NH_3 adsorption configurations, since adsorption can take place on one of the oxygen atoms in the structure (Acid Brønsted), or on one of the exposed vanadium atoms (Acid Lewis) (Zhao et al., 2020; Song et al., 2018). Furthermore, NH_3 can also adsorb on the support, whereby the NH_3 storage capacity increases by interaction with adjacent vanadium atoms (Song et al., 2020; Giraud et al., 2014).

Besides NH_3, DFT simulations showed that water can also adsorb on the catalyst surface by hydrogen bond interactions, with lower bonding energy than NH_3 (Ranea et al., 2000; Yin et al., 1999). This results in competition for adsorption sites with NH_3. Additionally, water can also dissociates into H^+ and OH^- which can activate sites for NH_3 adsorption (Wahab et al., 2008; Hejduk et al., 2010). As a result of the diversity of adsorption sites and water dynamics, a vanadium-based SCR catalyst has a broad operating range where the NH_3 storage capacity is stable.

Capturing the high diversity of NH_3 adsorption sites has been the objective of several models. The best NH_3 adsorption model in a vanadium-based catalyst used for SCR kinetics is the Temkin adsorption model (Lietti et al., 1997). In this model, adsorption is assumed to be non-activated (adsorption energy $E_a = 0$) and the desorption energy, E_d, decreases linearly with the coverage, θ, i.e. $E_d = E_d^o(1 - \alpha\theta)$ where E_d^o is the desorption energy at zero coverage and α is an empirical parameter describing the heterogeneity of the catalyst surface. However, the added parameter, α, does not have physical significance (Wang and Guo, 2020). Nova et al. proposed a modified Temkin model, where the desorption energy is expressed by two empirical parameters (α, σ) as $E_d = E_d^o(1 - \alpha\theta^\sigma)$ (Nova et al., 2006). While, Lietti et al. developed an empirical adsorption model assuming two adsorption sites with different acid strength and the desorption energy expressed as $E_d = E_d^o + B\tanh(-\alpha\theta + A)$, where A, B and α are empirical parameters (Lietti et al., 1997). The reviewed models assume a decrease of adsorption energy due to the interaction of adjacent adsorbates. However, commercial vanadium-based SCR catalysts are formulated with lower vanadium concentrations, i.e. below monolayer concentration (from 8 to 10 V/nm^2), which makes the adsorbate–adsorbate interaction unlikely (Wachs and Weckhuysen, 1997;

Haber et al., 1986). The lower concentration aims to increase the catalyst performance by active site – support interactions with the lowest amount of active material for economic purposes. Increasing the vanadium concentration (close to monolayer concentration) has been shown to be detrimental for NO_x conversion by previous studies (Djerad et al., 2004; Topsoe et al., 1995). Furthermore, with respect to NH_3 adsorption models for a vanadium-based SCR, there are no kinetic models which describe the effect of water and the catalyst oxidation state according to our knowledge.

In this study an NH_3 adsorption model for a vanadium-based SCR catalyst is developed using experimental adsorption isotherm data for a wide experimental region, considering different temperatures, NH_3 concentrations, water concentrations and catalyst oxidation states (oxidized and reduced). The present study explores a data-driven modeling process, aimed at maximising the information extracted from experimental data by developing computational and statistical methods that enable the evaluation of a large model candidate set.

From the data-driven modeling process, a single model is selected from several thousands of candidate models. The NH_3 adsorption model resulting from the proposed approach involves five adsorption sites with different adsorption mechanisms. This model describes the water dynamics and the influence of the catalyst oxidation state on the NH_3 storage capacity. Moreover, the obtained parameters from the model, ΔH_{ads} and ΔS_{ads}, have physical significance and fall within the range of values obtained from DFT calculations.

2. Methodology

2.1. Experimental Data

Ammonia adsorption isotherms over a wide experimental region were obtained for a state-of-the-art vanadium-based SCR catalyst using a gas flow reactor and a data preprocessing method developed for this study as described in our previous work (Suarez-Corredor et al., 2021). The experimental data were obtained under different conditions: two catalyst states (oxidized and reduced), three water concentrations (0.0%, 0.5% and 5.0%), different temperatures (100 to 250°C for the oxidized sample and 100 to 400°C for the reduced sample), and different NH_3 gas concentrations (from 0 to 500 ppm). The acquired NH_3 adsorption isotherms have features aimed to be included in the developed model: the different water dynamics for the oxidized and reduced catalyst, and the different saturation levels at different temperatures which suggest multiple adsorption sites over the catalysts.

2.2. Data-driven adsorption model

The proposed data-driven modeling framework aims for the maximization of information extracted from experimental data for inference about the adsorption nature in a vanadium-based SCR catalyst. The framework involves the evaluation of different model structures besides the parameters for the model since the model structure is a variable that can be tuned by adsorption mechanisms which describes the NH_3 adsorption isotherms. The modeling framework is an intensive optimization problem since the optimal parameters are evaluated for each model structure in a large set of adsorption model candidates. Then, the best model is chosen among the candidates by evaluating different criteria, such as fitting performance and low correlation between parameters. Furthermore, the data was divided into two workflows based on the catalyst oxidation state, improving the parameter estimation since opposite conditions, such as the oxidized and reduced catalyst state, could hinder the global optimum. The proposed modeling framework and its stages are presented in Fig. 1.

2.2.1. Multi-site adsorption model

The adsorption model in this work assumes that there are M different types of adsorption sites where NH_3 can adsorb. The total amount of NH_3 adsorbed in the catalyst is expressed as the sum over these M sites:

$$q_{NH_3} = \sum_{j=1}^{M} N_j \theta_j^{NH_3} \tag{1}$$

Where q_{NH_3} is the total amount of NH_3 adsorbed on the catalyst in mol $NH_3/g_{washcoat}$, N_j is the amount of sites of type j in mol/$g_{washcoat}$ and $\theta_j^{NH_3}$ is the NH_3 coverage of the site j. Each site is assigned an NH_3 adsorption mechanism, that form the building blocks for the global adsorption model structure for the catalyst. In this work,

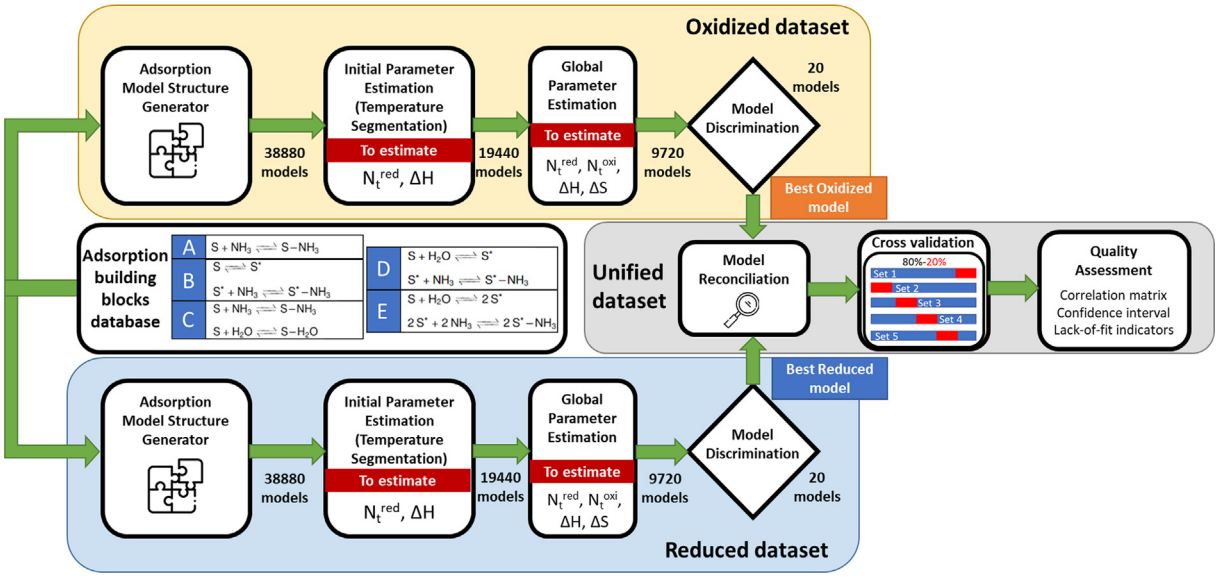

Fig. 1. Data-driven modeling framework for evaluation and discrimination of NH_3 adsorption models.

we considered five different adsorption mechanisms that each site can assume as listed in Table 1. The five mechanisms capture the possibilities how NH_3 and water interact with the catalytic surface and the transformation of sites between non-active and active state for NH_3 adsorption.

The adsorption mechanisms were motivated by the most likely and simplest interactions between an adsorption site with NH_3 and water, which are supported by previous studies at molecular scale (Ranea et al., 2000; Yin et al., 1999; Wahab et al., 2008; Hejduk et al., 2010; Topsoe et al., 1995). The adsorption mechanism include (See Table 1): Simple adsorption (A), which assumes NH_3 as the only compound to be adsorbed over the adsorption site and water does not have an effect on the NH_3 storage capacity; Site activation (B) where an adsorption site transforms into non-active and active site for NH_3 adsorption; Competitive adsorption (C), where NH_3 and water compete for adsorption sites; Water activated adsorption (D) which considers an adsorption site is activated by water and produces a single site for NH_3, increasing the overall NH_3 storage capacity; and Site duplication (E), which is similar to water activated adsorption but produces two sites for NH_3 adsorption.

The expressions for the coverage for each mechanism are derived within the framework of the Langmuir adsorption model. At equilibrium, the coverages can be expressed in terms of the equilibrium constant, K_c, describing the ratio of adsorption and desorption rate coefficients. Assuming ideal gases, the equilibrium constant, K_c, can be converted to the dimensionless thermodynamic equilibrium constant, K, by Eq. (2), allowing to relate the adsorption–desorption equilibrium to the Gibbs free energy change, ΔG, between the gas molecule and its adsorbed state as shown in Eq. (3).

$$K = K_c\left(\frac{RT}{P_{ref}}\right)^{\delta} \tag{2}$$

$$RT\ln(K) = -\Delta G \tag{3}$$

In Eq. (2) and (3), T is the temperature in K, R is the ideal gas constant, P_{ref} is the experiment total pressure (101.325 kPa), and δ is the sum of the stoichiometric coefficients for the gas phase species. The Gibbs free energy, ΔG, can be expressed in terms of the adsorption enthalpy change, ΔH_{ads}, and the adsorption entropy change, ΔS_{ads}, which leads to a relation for K as presented in Eq. (4). In that way, ΔH_{ads} and ΔS_{ads} become parameters to be estimated in the model evaluation process.

$$K = exp\left(\frac{-\Delta H_{ads} + T\Delta S_{ads}}{RT}\right) \tag{4}$$

Previous studies suggest that the molecular arrangement of adsorbed NH_3 and water is similar between the different adsorption sites of a vanadium-based SCR catalyst (Yin et al., 1999; Song et al., 2018; Ranea et al., 2000; Yin et al., 1999). This motivated to treat ΔS_{ads} as a global parameter, shared between the different adsorption sites and only specified by the type of reaction. Four different ΔS_{ads} values were assigned: ΔS_A for adsorbed NH_3, ΔS_W for adsorbed water, ΔS_S for site activation, and ΔS_D for site duplication. Furthermore, the number of adsorption sites of type j, N_j, is assumed to be different for the oxidized and reduced catalyst, defining two parameters as N_j^{red} for the total amount of sites of type j in the reduced catalyst and N_j^{oxi}, for the total amount of sites of type j in the oxidized catalyst.

2.2.2. Model structure generator and parameter estimation workflow

In a data-driven model development workflow, different model candidates are needed for a proper model discrimination process. The set of model candidates should be large enough to include the different feasible models for describing the data based on previous knowledge, but it should not be too large so it become infeasible by the current computing capabilities. Therefore, a model structure generator was developed for defining the possible combinations between the five adsorption mechanisms assuming the vanadium-based SCR catalyst comprises up to six types of adsorption sites (M = 1 to 6). For instance, if there is only one type of site (M = 1), there are 5 possible adsorption models (each having one of the mechanisms A to E in Table 1). For M = 2, there are 15 possible adsorption models, namely AA, AB, AC, ..., EE (in the case where the two sites follow the same mechanism, such as AA, the two sites are characterized by a different set of parameters). Hence, for M = 1, ..., 6, and five adsorption mechanisms (r = 5), there are 461 possible models obtained from the combination arrangement without repetition presented in Eq. (5).

$$C_{M,r} = \binom{M+r-1}{r-1} = \frac{(M+r-1)!}{(M-1)!r!} \tag{5}$$

Where $C_{M,r}$ is the number of models with up to M sites and r mechanisms. The parameter estimation workflow was performed in three steps using the three different objective functions presented in Table 2. At each step, 50% of the model candidates were passed over to the next step. The first step aimed for parameter initialization for which we assigned to each mechanism a certain subset of data and used the least square sum (LSS) function (see Table 2) as objective function for estimating the parameters for each mechanism. This step was repeated several times using different subsets of the data for each mechanism. This results in over 38,000 parameter estima-

Table 1
Site specific adsorption mechanisms forming the building blocks of the adsorption model.

Mechanism			Coverage
A	Simple Adsorption	S + NH_3 ⇄ S-NH_3	$\theta = \frac{K_{cA}C_A}{1+K_{cA}C_A}$
B	Site Activation	S ⇄ S*	$\theta = \frac{K_{cS}K_{cA}C_A}{1+K_{cS}+K_{cA}C_A}$
		S* + NH_3 ⇄ S*-NH_3	
C	Competitive adsorption	S + NH_3 ⇄ S-NH_3	$\theta = \frac{K_{cA}C_A}{1+K_{cW}C_W+K_{cA}C_A}$
		S + H_2O ⇄ S-H_2O	
D	Water activated adsorption	S + H_2O ⇄ S*	$\theta = \frac{K_{cW}K_{cA}C_AC_W}{1+K_{cW}C_W+K_{cW}K_{cA}C_AC_W}$
		S* + NH_3 ⇄ S*-NH_3	
E	Site duplication by water	S + H_2O ⇄ 2S*	$\theta = \frac{K_{cD}K_{cA}C_AC_W}{1+2K_{cD}C_W+2K_{cD}K_{cA}C_AC_W}$
		2S* + 2NH_3 ⇄ 2S*-NH_3	

Note. S = Adsorption site, S*=Activated adsorption site. Concentration (C_i) units in mol/m^3
Subscripts: A = Ammonia, W = Water, S = Surface activation, D = Site duplication

Table 2
Error function used as objective functions in parameter estimation

Error function	Nomcltr.	Equation
Least square sum	LSS	$LSS = \sum_{i=1}^{n} (q_{mod} - q_{exp})_i^2$
Marquardt's function	MSD	$MSD = \frac{1}{n-p} \sum_{i=1}^{n} \left[\frac{q_{exp} - q_{mod}}{q_{exp}}\right]_i^2$
Slope Tracking	ST	$ST = \frac{1}{n-p} \left[\lambda \sum_{i=1}^{n} \frac{[q_{exp} - q_{mod})]_i^2}{q_{exp,i}^2} + (1-\lambda) \sum_{j=1}^{m} \frac{[\alpha_{exp} - \alpha_{mod})]_j^2}{\alpha_{exp,j}^2}\right] + ln\left[\lambda \sum_{i=1}^{n} \frac{[q_{exp} - q_{mod})]_i^2}{q_{exp,i}^2} - (1-\lambda) \sum_{j=1}^{m} \frac{[\alpha_{exp} - \alpha_{mod})]_j^2}{\alpha_{exp,j}^2}\right]^2 ; \alpha = \frac{\Delta q}{\Delta C}|_T$

Note. n = Sample size, p = Number of parameters, m = Slope set size, α=Adsorption isotherm slope
λ=Contribution factor, q = NH_3 adsorption capacity

tion assignments to be evaluated in the first step (See Fig. 1). In the second step, around 19,000 parameter estimation assignments were considered using the Marquardt's objective function, which includes more information in the objective function for model discrimination since it normalizes the residual over the experimental region and weights the sample size, n, with the number of parameters, p. Finally, a fine tuning was performed in the third step by using the slope tracking function (see Table 2), a custom-made function including the slope, α, evaluated at three specific locations along an isotherm curve. The slope tracking function includes a new parameter, λ, which aims to balance the contribution between the normalized sum of residual (first term in the first bracket) and the normalized sum of the slope's difference (second term in the first bracket). The logarithmic term added to the slope tracking function presents a reward term for fulfilling the equal contribution constraint (Griva et al., 2009). Moreover, the logarithmic function amplifies the reward effect for an objective function already close to the optimal solution. Including this term adds additional constraints to the objective function, improving convergence and separating noise from usable information in the data. In this step over 9,000 parameter estimation assignments were evaluated.

For the NH_3 adsorption model development, two different workflows were performed: one workflow for the reduced dataset with all the NH_3 adsorption isotherm data for the reduced catalyst state, and another for the oxidized dataset, with the isotherms for the oxidized catalyst state (See Fig. 1). Each workflow generated a set of around 9,000 model candidates which were evaluated and unified in the next stage of the data-driven model development process.

2.2.3. Model discrimination and reconciliation

In this stage, the 20 best models from each parameter estimation workflow were chosen for a more detailed model discrimination process. A small but representative model set facilitates the visualization of the different criteria used in model discrimination. First, the Akaike information criterion (AIC) presented in Eq. (6) was used for the evaluation of the model performance. The AIC evaluates lack-of-fit weighted by the number of parameters in the model (Anderson and Burnham, 2004).

$$AIC = n \cdot \log\left(\frac{1}{n}\sum_{i=1}^{n}\left[\frac{q_{exp} - q_{mod}}{q_{exp}}\right]_i^2\right) + 2(p+1) \tag{6}$$

Furthermore, an overfitting assessment was performed by the evaluation of the pair-wise correlation between parameters. The pair-wise correlation was estimated using the methods for linear models which can be extended to non-linear models since a small perturbation in the parameters for estimating the Jacobian can be assumed to have a linear behavior.

From each workflow, oxidized and reduced, the best model with the lowest AIC value and the lowest correlation distribution between parameters was chosen. These two models were then used for building a unified adsorption model in the reconciliation step. A unified model was created by integrating the similarities and differences between the models. A common set of parameters for each site type was defined for the similar adsorption site types between the oxidized and reduced model, while a separate set of parameters was defined for the adsorption type sites that differed between the oxidized and reduced catalyst. The values from the previous parameter estimation workflows were used as initial estimates and the Slope tracking objective function was used for parameter estimation. The result from this step is a unified adsorption model with an optimal set of parameters, which minimizes the error between the model and experimental data. However, the optimal set of parameters depends on the specific dataset and a robust model should not be affected by the uncertaintites on the dataset. Therefore, a cross-validation step was performed for estimating a robust set of parameters.

A k-fold cross-validation method was used, where the full dataset was divided randomly into k subsets equally distributed (k = 5 for this study). The model parameters were estimated k times using the optimal set of parameters in the unified model as initial values (Airola et al., 2011; Kuhn et al., 2013). Each time, one subset was assigned to the validation set, and, $k-1$ subsets were used for parameter estimation. The robust set of parameters for the unified model was estimated as the mean value of the obtained parameters at each of the k steps. Then, a quality assessment for the unified model with robust parameters was performed. The quality assessment involves the estimation of the correlation matrix and the confidence interval for the parameters. Furthermore, lack-of-fit indicators were evaluated such as LSS, AIC and adjusted R^2. Finally, a local residual analysis, presented in Supplementary Material, was implemented to identify zones in the experimental region which could benefit from an additional experimental effort.

3. Results

The best NH_3 adsorption model selected from the data-driven modeling process is a 5-site model which comprises of a single site with a simple adsorption mechanism, three sites with a competitive adsorption mechanism with water, and one site with a water activated adsorption mechanism as outlined in Table 3. Fig. 2 shows the fitting performance of the developed model using the parameter values listed in Table 3 (continuous lines) compared with the experimental data (black circles).

The main features from the experimental data are properly captured: the difference in NH_3 storage capacity between the reduced and oxidized catalyst; the water dynamics for the reduced catalyst which lowers the NH_3 storage capacity; and the water dynamics of the oxidized catalyst which increases the NH_3 storage capacity at low water concentration (0.5%) and decreases at high water concentration (5.0%). This dynamic is described as a significant effect of the activated adsorption site at low water concentration

Table 3
Ammonia adsorption model mechanisms structure and parameters with confidence interval.

	S_j-N^{red}s (mol/g_{wash})	S_j-N^{oxi} (mol/g_{wash})		Mechanism	ΔH_{ads} (kJ/mol)	ΔS_{ads} (J/mol.K)
Site 1	3.26E-05 ± 6.86E-07	2.92E-05 ± 5.94E-07	**A**	$S + NH_3 \rightleftarrows S\text{-}NH3$	−109.91 ± 7.6	−173.58 ± 2.8
Site 2	2.03E-05 ± 5.10E-07	4.85E-05 ± 1.05E-06	**C**	$S + NH_3 \rightleftarrows S\text{-}NH_3$	−155.25 ± 1.2	−173.58 ± 2.8
				$S + H_2O \rightleftarrows S\text{-}H_2O$	−91.73 ± 1.2	−100.59 ± 1.7
Site 3	2.90E-05 ± 5.54E-07	2.58E-05 ± 1.08E-06	**C**	$S + NH_3 \rightleftarrows S\text{-}NH_3$	−127.98 ± 9.4	−173.58 ± 2.8
				$S + H_2O \rightleftarrows S\text{-}H_2O$	-130.08 ± 4.9	-100.59 ± 1.7
Site 4	4.29E-05 ± 8.20E-07	4.18E-05 ± 5.94E-07	**C**	$S + NH_3 \rightleftarrows S\text{-}NH_3$	−95.56 ± 6.3	−173.58 ± 2.8
				$S + H_2O \rightleftarrows S\text{-}H_2O$	−49.03 ± 1.0	−100.59 ± 1.7
Site 5	1.89E-05 ± 4.46E-07	4.80E-05 ± 1.05E-06	**D**	$S + H_2O \rightleftarrows S^*$	−60.96 ± 2.3	−100.59 ± 1.7
				$S^* + NH_3 \rightleftarrows S^*\text{-}NH_3$	−153.56 ± 6.4	−173.58 ± 2.8

Note. S_j-N^{red} = Adsorption sites density for site *i* in the reduced catalyst, S_j-N^{oxi} = Adsorption sites density for site *i* in the oxidized catalyst, ΔH_{ads} = Adsorption enthalpy change, ΔS_{ads} = Adsorption entropy change.

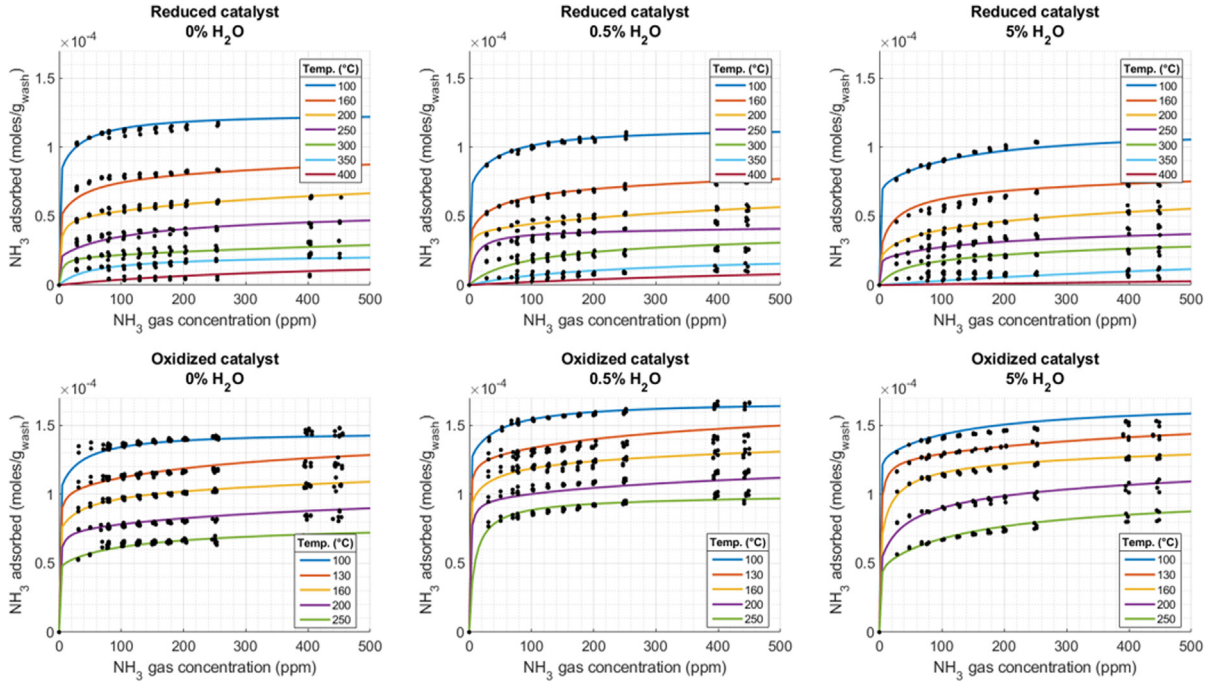

Fig. 2. Ammonia adsorption model fitting performance for the experimental adsorption isotherms. Continuous line = model values. Black circles = experimental data.

(0.5%), while at higher water concentration (5.0%) competitive adsorption becomes more relevant and reduces the total amount of NH_3 adsorbed. Another feature captured by the model is the different saturation levels at different temperatures which indicates multiple adsorption sites over the catalyst. Furthermore, the model fitting does not deviate from the experimental data over the experimental region, validating the wide application range of the developed model. The highest deviations were presented at low NH_3 concentrations and low temperatures without water, and at high NH_3 concentrations and low temperature with high water concentration (5.0%). Nevertheless, these deviations do not affect the overall fitting performance and the description of the main features in the experimental data.

In the model, the significance of the sites is indicated by the site density parameter for each site listed in Table 3. For the reduced catalyst the most important sites are: site 4 with a competitive adsorption mechanism followed by site 1 with a simple adsorption mechanism. On the other hand, for the oxidized catalyst, the most significant sites are site 2 with a competitive adsorption mechanism and site 5 with a water activated adsorption mechanism, which is not relevant for the reduced catalyst. Furthermore, sites 1, 3 and 4 have similar parameter values for the reduced and oxidized catalyst, indicating that these sites are not affected by the catalyst oxidation state in contrast to sites 2 and 5. Fig. 3 summarizes the difference in the adsorption sites between the oxidized and reduced catalyst state.

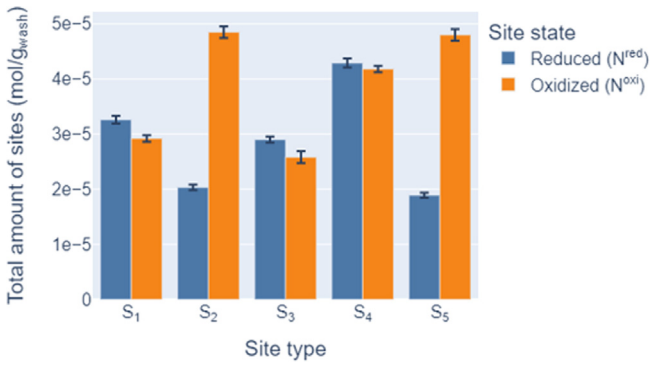

Fig. 3. Amount of adsorption sites for each site type for the reduced catalyst, N^{red} (blue bar), and the oxidized catalyst, N^{oxi} (orange bar) obtained from the developed model.

The adsorption enthalpies, ΔH_{ads}, for NH_3 and water for each site are presented in Table 3. The NH_3 adsorption enthalpy varies from −95 to −155 kJ/mol, and the water adsorption enthalpy ranges from −49 to −130 kJ/mol. For most of the sites, water adsorption has a lower enthalpy than NH_3 in agreement with previous studies (Yin et al., 1999; Song et al., 2018; Ranea et al., 2000; Yin et al., 1999). However for site 3, the adsorption enthalpies for NH_3 and water have similar values, −127 and −130 kJ/mol, respectively. This suggests an adsorption configuration with similar bonding strength which is not the case for adsorption over a Brønsted or Lewis acid site for which NH_3 is a stronger base than water.

The enthalpies obtained for the NH_3 adsorption model are within the range of values reported for vanadium and titanium oxide clusters obtained in DFT studies. Fig. 4 shows the adsorption enthalpy from the DFT studies together with the parameters obtained in this work. The adsorption enthalpy from the DFT studies has a wide range since vanadium has different structures in the catalyst surface interacting with the support or promoters. The NH_3 enthalpy values for titanium oxide clusters have lower spread than the values for vanadium, but the water enthalpy values show more variation since water dissociates over vanadium and titanium oxides. The obtained values from the model are within the expected range compared to the DFT simulations increasing the validity and physical significance of the model.

With respect to the adsorption entropy, ΔS_{ads}, only two global variables were required by the model: ΔS_A with a value of −173 J/mol.K for NH_3, and ΔS_W with a value of −100 J/mol.K for water. For verification, the transition-state theory was used to estimate the limiting values for the adsorption entropy by treating NH_3 and H_2O as a two-dimensional adsorbed molecule and as a completely localized species (See supplementary material). The obtained values for the model are within the range of these extreme cases. These values suggest that NH_3 adsorption is highly localized, with the NH_3 molecule losing most of its degrees of freedom while for water adsorption, the water molecule keeps some mobility over the catalytic surface which is believed to be relevant for activating sites for NH_3 adsorption.

The confidence intervals (α=0.95) for the model parameters are small as presented in Fig. 5. The normalized confidence interval for each parameter is less than 5% in most of the cases while for the adsorption enthalpy, ΔH, on sites 1, 3 and 4 it can reach around 7% of the optimum value. Nevertheless, these parameters are still significant and the intersection between the different confidence intervals is minimal.

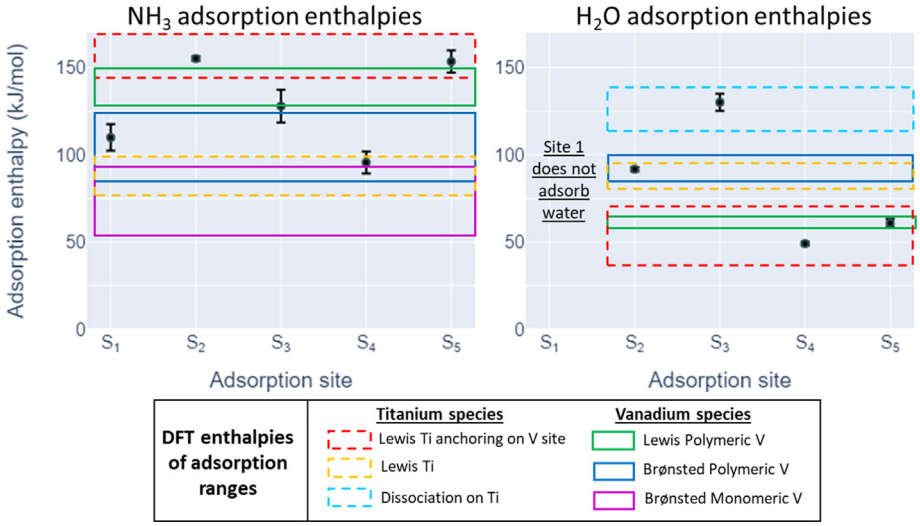

Fig. 4. Adsorption enthalpy, ΔH_{ads}, comparison between DFT studies for vanadium and titanium clusters, and the obtained values from the proposed model (Giraud et al., 2014; Vittadini et al., 2005; Ranea et al., 2000; Hejduk et al., 2010; Wahab et al., 2008; Yin et al., 1999).

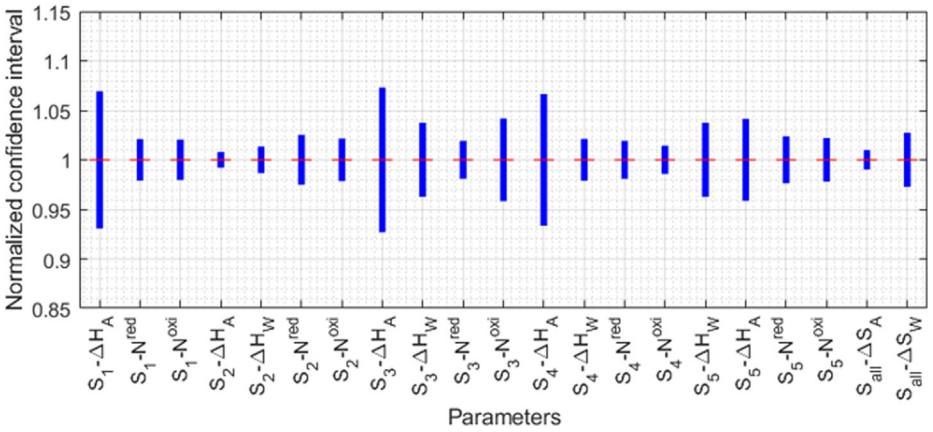

Fig. 5. Normalized 95% confidence interval for the model parameters (the dimensional confidence interval is divided by the actual value of each parameter).

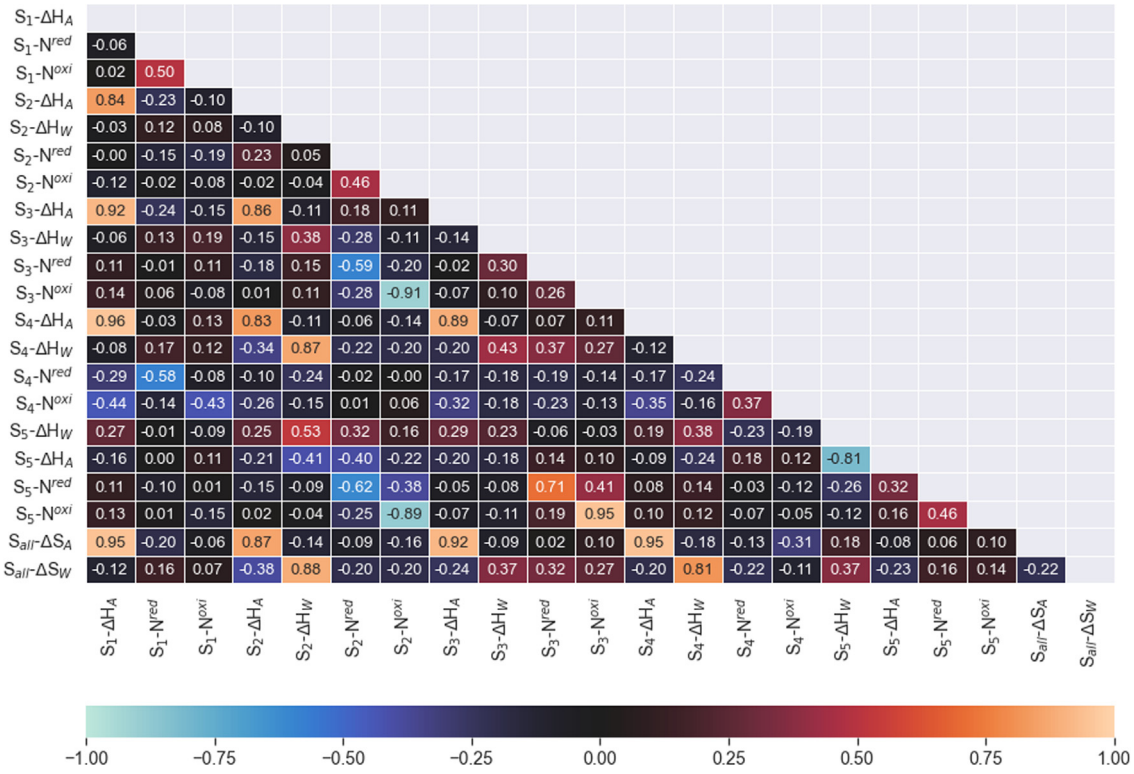

Fig. 6. Correlation matrix for the selected NH_3 adsorption model.

Fig. 6 shows the correlation matrix for evaluating the parameter interaction for the selected NH_3 adsorption model. Each cell in the correlation matrix evaluates the interaction between each pair-wise parameter combination from −1 to 1. The correlation values can be related to the microscopic behavior of the catalyst for making inferences. High correlations are expected since the proposed NH_3 adsorption model is highly non-linear but values closer to the limit, −1 or 1, should be analyzed individually since they can be a sign of model overfitting. Overfitting is reduced by selecting a model with fewer parameters.

For the selected NH_3 adsorption model, correlation values are low for most of the pair-wise combinations; the few high values (around 0.80-0.96) do not represent overfitting since the confidence intervals for the parameters are small. Nevertheless, they revealed expected interactions in a non-linear model. For instance, NH_3 adsorption entropy, ΔS_A (second last row in Fig. 6), has a high correlation with all the NH_3 adsorption enthalpies, and water adsorption entropy, ΔS_W (last row in Fig. 6), has a high correlation with all the water adsorption enthalpies. This is expected due to the relationship between ΔS and ΔH when estimating the dimensionless thermodynamic equilibrium constant, K, see Eq. (4).

In the case of the amount of adsorption sites in the catalyst, a high negative correlation is observed between sites 5 and 2 (−0.89 for the oxidized catalyst and −0.62 for the reduced catalyst). The high negative correlation implies that a positive change in one of the parameters corresponds to a negative change of the other one in order to preserve the model behavior. Therefore, an increase of type 2 adsorption sites with a competitive adsorption mechanism, reduces the adsorption of type 5 sites with the water activated adsorption mechanism. Furthermore, a high negative correlation is identified between the sites 3 and 2 (−0.91 for the oxidized catalyst and −0.59 for the reduced catalyst). Both sites have a competitive adsorption mechanism but with different adsorption enthalpies. The high correlation is observed for the oxidized catalyst at low temperatures (100-250°C), where both sites have a similar effect over the NH_3 coverage. However, for the reduced catalyst, there is a wider experimental temperature range, where these sites can be differentiated. Likewise, there is a high correlation between the amounts of adsorption sites 5 and 3 (0.95 for the oxidized catalyst and 0.71 for the reduced catalyst), justified by the interplay between a site with a competitive adsorption mechanism and a site with water activated adsorption mechanism and their opposite outputs on the NH_3 storage capacity. This is explained by dynamic interactions between vanadium species and neighboring species such as the support or the promoters. For site 3 and 5, if the amount of one site is increased (competitive adsorption), it will increase the amount of neighboring species as well (activated adsorption). This effect on the amount of sites keeps the catalyst adsorption nature captured by the model.

In the case of adsorption enthalpies, ΔH, a negative high correlation is detected between the NH_3 adsorption enthalpy in site 5, and the water enthalpy of the same site (−0.81). For site 5 water is required to activate the site for NH_3 adsorption. Therefore, as the water adsorption enthalpy is reduced, less sites will be activated by water and the NH_3 adsorption enthalpy would increase to compensate and achieve the same NH_3 coverage magnitude. Stronger interactions with NH_3 occur as a result of the increase of available space over the adsorption site since water molecules bind more weakly. Moreover, sites 2 and 4 are highly correlated for the NH_3 and water adsorption enthalpy (0.83 and 0.87 respectively). The high correlation is explained by the same mechanism in site 2 and 4 where NH_3 is strongly adsorbed compared to water. The sites could be related to similar species over the catalyst interacting with the support. As a consequence of the similar nature, an increase in the adsorption strength in one of the sites, will increase the same parameter at the other site. Finally, all NH_3 adsorption enthalpies are positively correlated between each other with values ranging from 0.84 to 0.96. This reflects the complexity over the catalyst surface where all the adsorption sites have an impor-

tant influence in the total NH_3 adsorbed. The different NH_3 adsorption enthalpies are close between each other, making the site differentiation a challenge if not enough diverse information is provided by the experimental data resulting in high correlations and wide confidence intervals as presented in Fig. 5.

4. Discussion

The data-driven modeling process proposed in this study involves the evaluation of a large set of candidate models that were generated systematically by combining the adsorption site types assumed on the catalyst and a feasible set of adsorption mechanisms aimed to describe the main features of the experimental data. Moreover, the parameter estimation was performed with multiple initial values to avoid local optima, and the data was distributed among the site types to obtain a fast initial solution which was fine tuned at later stages. As a result, around 38,000 parameter estimation assignments were evaluated in the first step of the parameter estimation workflow. Then, 50% of the best solutions were chosen for the second step (over 19,000) using a different objective function. Finally, half of the best solutions (approx. 9,000) were selected for the third parameter estimation step using the slope tracking objective function developed for this study.

The fitting performance evolution for each workflow, reduced and oxidized, in the different parameter estimations steps is presented in Fig. 7. Each parameter estimation assignment is a point in the figure where the Akaike information criterion was calculated as a reference for model discrimination. The red points represent the solutions that were selected for the next step. Even though only 50% of the candidates were chosen for the next step, it is noticed that the selected model set was representative since most of the assumed site types (1 to 6) were included.

The high spread of the AIC value as an indicator of fitting performance in all the three steps confirms the highly non-linear nature of the NH_3 adsorption model and the challenge on avoiding local minima solutions. This supports the need to create a large candidate set and multiple initialization states for reaching a global minima and maximizing the usable information from data. Each step contributes on improving the fitting performance and the effect is substantial for the oxidized workflow, where the best models had an AIC value around −3,500 in the first step and in the last step the AIC value for the best models is approx. −10,000. On the other hand, for the reduced workflow, the fitting improvement is smaller evolving from an AIC of −2,000 in the first step to −5,550 in the third step. The difference in magnitude could be explained as the differences in the reduced and oxidized dataset size (n = 875 and n = 960 respectively) and the smaller NH_3 adsorption values for the reduced state catalyst compared to the oxidized one. As the NH_3 adsorption values are smaller, the deterministic fraction attempted to be described by the model and the fitting performance are reduced. However, the AIC change in the third step shows the higher impact due to the slope tracking objective function, which has additional constraints improving convergence, specially when the experimental region is broad.

Another relevant aspect from Fig. 7 is the differentiation of a set of model candidates from the second step, with better AIC values than the rest of models. This is the result of achieving global optima solutions for different model structures, which is one of the main purposes of parameter estimation. In the last step, the 20 best models were chosen (red points in the third column of Fig. 7). By magnifying the scale as displayed in panel a) and panel b), a 5-site adsorption model has the best fitting performance for the reduced and oxidized workflow, followed by a 6-site adsorption model. The AIC difference between the first and second best model is around 20 for the reduced workflow and around 23 for the oxidized workflow. Based on the heuristics provided for the AIC method for model discrimination, a difference larger than 10 makes the second best model not significant (Anderson and Burnham, 2004). This supports that increasing the number of site types to 6 will not improve the fitting performance, with an unstable behavior due to overfitting. Moreover, the AIC value favours

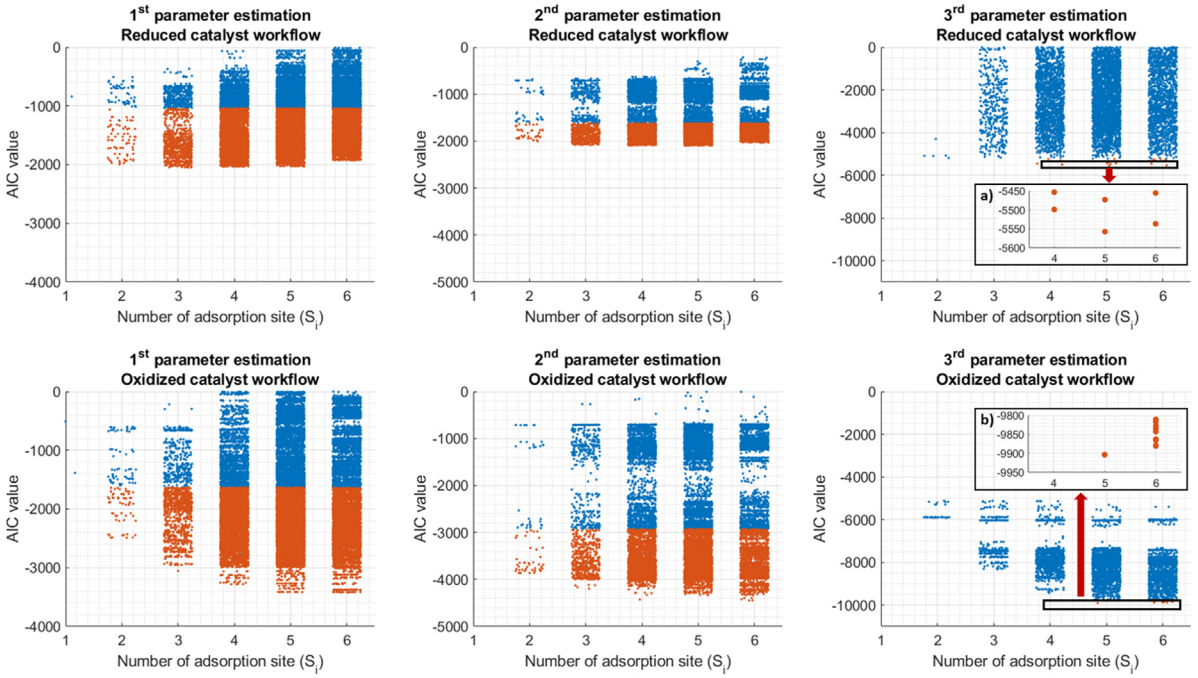

Fig. 7. Fitting performance of the three parameter estimation steps, evaluated by the AIC indicator (columns) for the workflow of the reduced (top row) and oxidized (bottom row) catalyst state. Points represent parameter estimation assignments. Red points are the solutions used in the next step. Panel a) and b) in the third column show a magnified view for the best models region.

Table 4
Fitting performance summary for the 20 best models in the oxidized and reduced workflow, by the least square sum (LSS), the Akaike information criterion (AIC) and Marquardt objective function.

Reduced catalyst workflow

Model ID	Mechanism	p	LSS	AIC	Marquardt
1	ACAAC	20	50.52	-5557.07	0.239
2	BACCAC	25	50.79	-5536.37	0.242
3	BDCB	19	52.25	-5498.59	0.246
4	CCAEB	23	52.53	-5472.81	0.250
5	BCCCBB	27	52.60	-5455.19	0.246
6	BDCA	18	53.56	-5453.08	0.248
7	ABCBA	21	53.64	-5440.07	0.249
8	BBCDC	23	53.58	-5432.46	0.336
9	BDCDC	23	55.06	-5376.95	0.319
10	AACECC	25	55.80	-5344.84	0.245
11	BCCDC	23	56.11	-5338.54	0.285
12	AACECB	26	56.27	-5322.81	0.244
13	BDCCBE	28	56.35	-5309.95	0.254
14	ABCDAC	25	57.05	-5300.11	0.253
15	BCCDBD	27	56.82	-5298.04	0.267
16	ABCC	18	57.90	-5295.02	0.257
17	ABCABE	26	58.12	-5257.02	0.254
18	BECCDE	28	58.19	-5244.75	0.387
19	BDCCBE	19	59.22	-5244.05	0.262
20	ABCAD	21	59.27	-5237.24	0.438

Oxidized catalyst workflow

Model ID	Mechanism	p	LSS	AIC	Marquardt
1	AACCD	20	0.56	-9903.22	0.194
2	BCCCD	23	0.57	-9880.21	0.196
3	ABCDCC	26	0.57	-9879.20	0.201
4	CCCEAA	25	0.58	-9865.17	0.199
5	CCCEBB	28	0.57	-9862.41	0.198
6	CCDCA	21	0.58	-9842.40	0.202
7	CBCCAD	26	0.59	-9841.81	0.200
8	CCBDC	23	0.59	-9833.96	0.203
9	CCCDAE	26	0.59	-9827.71	0.201
10	CECACA	25	0.60	-9816.43	0.201
11	CCCADB	26	0.60	-9810.65	0.203
12	CBCDC	23	0.60	-9797.98	0.203
13	CCCAD	21	0.61	-9797.23	0.199
14	BDDCCC	27	0.61	-9790.50	0.201
15	ACCBEC	27	0.61	-9783.93	0.207
16	CCCEAB	27	0.61	-9783.58	0.209
17	CCCAEA	25	0.62	-9775.96	0.238
18	CCCEBA	27	0.62	-9773.55	0.237
19	CCEBC	24	0.62	-9761.34	0.236
20	CBCCE	24	0.62	-9759.58	0.249

models with fewer parameters if they provide adequate fitting performance.

For a detailed model discrimination, the 20 best models for each workflow are summarized in Table 4. The AIC indicator shows similar behavior as the least square sum values, but the AIC provides better resolution for model discrimination and penalizes model complexity. The three objective functions, LSS, AIC and the Marquardt objective function, determine the same best model, but the model ranking is different for the Marquardt objective function compared to the AIC and LSS model rankings. This shows how the number of parameters, p, and the sample size, n, are used different in each function affecting the results on model discrimination.

Regarding the number of parameters, p, the best model for the oxidized and reduced workflow has 20 parameters. Another model with more parameters was also among the 20 best models, with lower fitting performance. This confirms that the selected models do not have overfitting issues, and the model discrimination balances fitting performance and model complexity. Additionally, the correlation matrix was calculated for all the candidates and the distribution of all pair-wise correlation values for the reduced and oxidized workflow is presented in Fig. 8.

The model with the best fitting performance with no overfitting has low values (close to zero) on the pair-wise parameter correlations. However, some high values are expected since the adsorption model is non-linear and some parameters are inherently

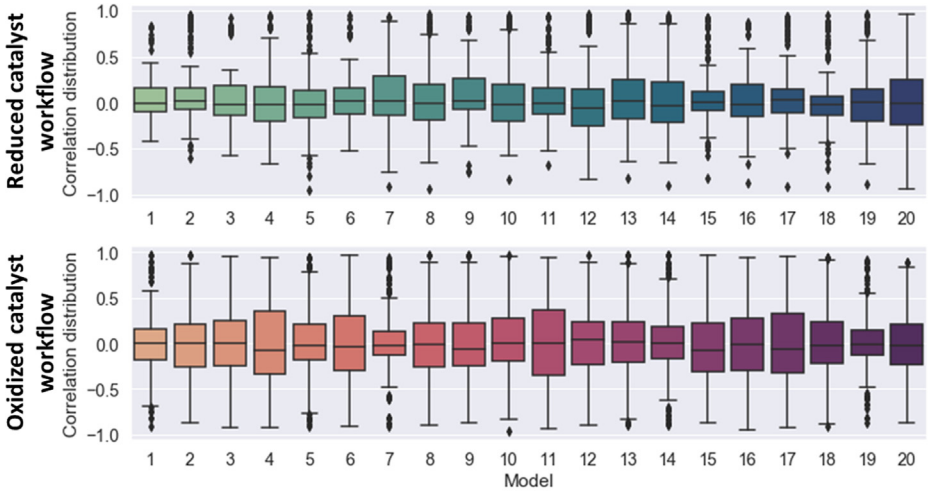

Fig. 8. Pair-wise parameter correlation distribution for the 20 best models in the oxidized and reduced workflow.

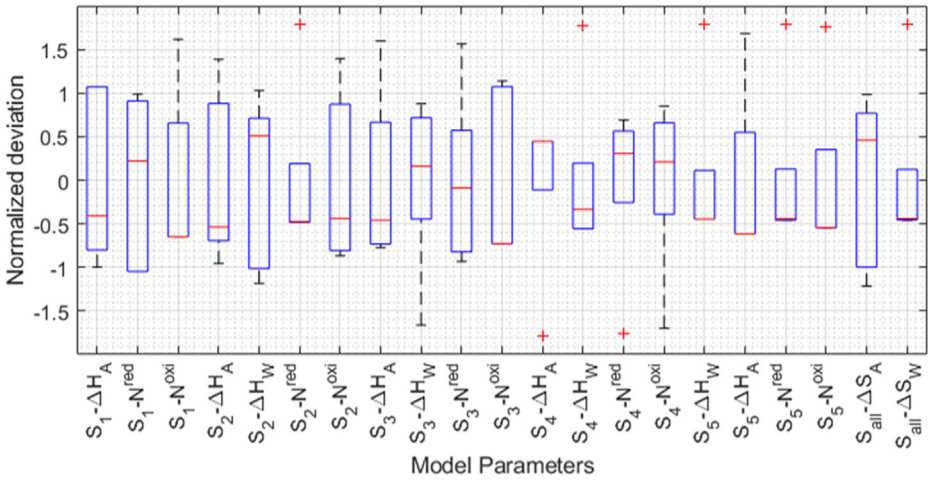

Fig. 9. Cross-validation results with the parameter variation at each scenario. The red line in each bar represents the mean value used as the final value for the unified robust model. A standard normalization presents the deviations in terms of the standard deviation (σ).

correlated (ΔH and ΔS, see Eq. (4)). For the reduced and oxidized workflow, model 1 is one of the models with the lowest variance value of the correlation distribution. Even though for the oxidized workflow, model 7 and 19 may have more narrow correlation distribution compared to model 1, the fitting performance is the main indicator for model discrimination. From the model discrimination process, a 5-site adsorption model was chosen from the reduced workflow. This involves 3 sites with the NH_3 simple adsorption mechanism and 2 sites with the competitive adsorption mechanism. From the oxidized workflow, a 5-site adsorption model was selected, which includes 2 sites with an NH_3 simple adsorption mechanism, 2 sites with a competitive adsorption mechanism and one site with the water activated adsorption mechanism.

In the reconciliation step, a unified adsorption model is built by identifying the similarities from the two models obtained in the oxidized and reduced dataset workflow. The following similarities were identified: an adsorption site with the NH_3 simple adsorption mechanism and similar adsorption enthalpies. Furthermore, similar NH_3 adsorption enthalpies were found for one site with competitive adsorption in the reduced workflow model and one site with simple adsorption in the oxidized workflow model; as well as for two sites with simple adsorption in the reduced workflow model and two sites with competitive adsorption in the oxidized workflow model. For all these cases, the competitive adsorption mechanism was selected in the unified model since it captures the interactions with water.

Additionally, for the reduced workflow model, a site with competitive adsorption has similar adsorption enthalpies as the site with the water activated mechanism in the oxidized workflow model. Here, the water activated adsorption mechanism is chosen for the unified model since it is the only mechanism which describes NH_3 storage enhancement due to water. As a result of this rationale, the reconciliation step generated the chosen NH_3 adsorption model described earlier.

The distribution of the cross-validation scenarios is presented in Fig. 9. The box plot for each parameter shows the mean and standard deviation from the *k*-fold cross-validation, normalized by the parameter value of the original model obtained from optimizing the experimental data in the reconciliation step. The mean value is presented as the red line from each bar in the box plot. The mean value is calculated from the different values obtained from the cross-validation scenarios and they are used as the final values for the unified robust model. The spread of the values from the cross-validation scenarios are expressed by the bar size, its whiskers and the outliers (plotted with the '+' symbol). The parameters for the unified robust model are modified by less than 0.5 standard deviations (σ) with respect to the optimal model determined for the specific experimental data. As a result, the unified model from the cross-validation step provides a robust description accounting for data uncertainties while not changing the physical significance and interpretation of the optimal parameters obtained in the previous steps.

5. Conclusions

A 5-site NH_3 adsorption model for a vanadium-based SCR catalyst was developed by the use of a new data-driven modeling process using experimental adsorption isotherms data from a gas flow reactor setup. The adsorption isotherms were obtained at different temperatures, NH_3 concentrations, water concentrations and catalyst oxidation states. The model, developed within the Langmuir adsorption framework, consists of one site with simple NH_3 adsorption, three sites with competitive adsorption with water and one site with a water activated adsorption mechanism. As a result, the model captures the main features of the experimental adsorption isotherms: the different NH_3 storage capacities between the reduced and oxidized catalyst, the diverse saturation levels with temperature, and the water dynamics that reduces the NH_3 storage capacity due to competitive adsorption but can increase the capacity in the oxidized catalyst at low water concentrations (0.5%) as a result of site activation with water.

The model parameters include the adsorption enthalpy, ΔH_{ads}, and the adsorption entropy, ΔS_{ads}. They have physical significance since they are related to the molecule bonding strength with the catalytic surface and its spatial arrangement. The values for the adsorption enthalpy suggest that NH_3 and water adsorb on different adsorption sites over the catalytic surface with different strength. Moreover, water adsorbs weaker than NH_3 since it is a weaker base interacting with acidic adsorption sites (Brønsted and Lewis). However, for one of the sites the adsorption enthalpy between NH_3 and water has similar values which suggests another type of interaction. The NH_3 adsorption enthalpy ranges from -95 kJ/mol to -155 kJ/mol while the water adsorption enthalpy ranges from -49 kJ/mol to -130 kJ/mol which agrees with values reported from previous studies at molecular level.

The adsorption entropy indicates that the NH_3 adsorption is highly localized, with the molecule losing most of its degrees of freedom. On the other hand, water is a more mobile molecule over the catalyst surface with a more dynamic behavior that involves adsorption, dissociation, and activation. The five adsorption sites

have different behavior based on the catalyst oxidation state. Three adsorption sites are not affected by reduction (performed with NH_3 at high temperature, see previous work (Suarez-Corredor et al., 2021)) while for two sites, the NH_3 storage capacity increased considerably when oxidized. This indicates the presence of multiple adsorption sites where some of them do not need to be involved in the SCR reaction mechanism but serve as sites for NH_3 storage or buffer. Furthermore, it also suggests that NH_3 adsorbs also on the support and the different vanadium structures present over the catalytic surface experience different affinities towards reduction by NH_3. From the correlation matrix analysis, interaction between the sites was identified as a result of the interplay between the support, promoters and the vanadium structures over the catalytic surface.

The proposed data-driven method aims to maximize the utilisation of information from experimental data. This was achieved by considering the model structure as a variable prone to optimize and generating a set of models to be evaluated. The set of model candidates was generated systematically by combining feasible adsorption mechanisms with the assumed number of site types in the catalyst. A large set of candidates guarantees that suitable models are not neglected. Furthermore, a global optimum for all model candidates was achieved by a sequential parameter estimation workflow using different objective functions with increased complexity, improving convergence and fitting performance. Finally, the quality assessment based on different indicators and procedures, such as cross-validation, exemplifies the model validity and robustness.

CRediT authorship contribution statement

Andres Suarez: Conceptualization, Methodology, Software, Investigation, Writing – Original Draft, Visualization. **Matthäus Bäbler:** Conceptualization, Methodology, Writing - Original Draft, Supervision. **Louise Olsson:** Conceptualization, Writing – Review & Editing. **Magnus Skoglundh:** Conceptualization, Writing – Review & Editing, Funding acquisition. **Björn Westerberg:** Conceptualization, Methodology, Software, Resources, Writing – Original Draft, Supervision.

Declaration of Competing Interest

The authors declare that they have no known competing financial interests or personal relationships that could have appeared to influence the work reported in this paper.

Acknowledgement

This research project is sponsored by Scania CV AB. The Competence Centre for Catalysis is hosted by Chalmers University of Technology and financially supported by the Swedish Energy Agency and the member companies ECAPS AB, Johnson Matthey PLC, Perstorp AB, Powercell Sweden AB, Preem AB, Scania CV AB, Umicore Denmark AB, and Volvo Technology AB. The authors acknowledge Umicore for providing the catalyst samples.

Appendix A. Supplementary material

Supplementary data associated with this article can be found, in the online version, at https://doi.org/10.1016/j.ces.2022.117975.

References

Airola, A., Pahikkala, T., Waegeman, W., De Baets, B., Salakoski, T., 2011. An experimental comparison of cross-validation techniques for estimating the area under the ROC curve. Comput. Stat. Data Anal. 55 (4), 1828–1844.
Anderson, D., Burnham, K., 2004. Model selection and multi-model inference. Second. NY: Springer-Verlag 63 (2020), 10.
Anstrom, M., Dumesic, J., Topsøe, N.-Y., 2002. Theoretical insight into the nature of ammonia adsorption on vanadia-based catalysts for SCR reaction. Catal. Lett. 78 (1), 281–289.
Anstrom, M., Topsøe, N.-Y., Dumesic, J., 2003. Density functional theory studies of mechanistic aspects of the SCR reaction on vanadium oxide catalysts. J. Catal. 213 (2), 115–125.
Arnarson, L., Falsig, H., Rasmussen, S.B., Lauritsen, J.V., Moses, P.G., 2017. A complete reaction mechanism for standard and fast selective catalytic reduction of nitrogen oxides on low coverage VO_x/TiO_2 (001) catalysts. J. Catal. 346, 188–197.
Djerad, S., Tifouti, L., Crocoll, M., Weisweiler, W., 2004. Effect of vanadia and tungsten loadings on the physical and chemical characteristics of V_2O_5-WO_3/TiO_2 catalysts. J. Mol. Catal. A: Chem. 208 (1–2), 257–265.
Frey, H.C., 2018. Trends in on-road transportation energy and emissions. J. Air Waste Manage. Assoc. 68 (6), 514–563.
Giraud, F., Geantet, C., Guilhaume, N., Gros, S., Porcheron, L., Kanniche, M., Bianchi, D., 2014. Experimental microkinetic approach of de-NO_x by NH_3 on V_2O_5/WO_3/TiO_2 catalysts. 1. Individual heats of adsorption of adsorbed NH_3 species on a sulfate-free TiO_2 support using adsorption isobars. J. Phys. Chem. C 118 (29), 15664–15676.
I. Griva, S.G. Nash, A. Sofer, Linear and nonlinear optimization, Vol. 108, Siam, 2009.
Haber, J., Kozlowska, A., Kozłowski, R., 1986. The structure and redox properties of vanadium oxide surface compounds. J. Catal. 102 (1), 52–63.
Heck, R.M., Farrauto, R.J., Gulati, S.T., 2016. Catalytic air pollution control: commercial technology. John Wiley & Sons.
He, G., Lian, Z., Yu, Y., Yang, Y., Liu, K., Shi, X., Yan, Z., Shan, W., He, H., 2018. Polymeric vanadyl species determine the low-temperature activity of V-based catalysts for the SCR of NO_x with NH_3, Science advances 4 (11), eaau4637.
Hejduk, P., Szaleniec, M., Witko, M., 2010. Molecular and dissociative adsorption of water at low-index V_2O_5 surfaces: DFT studies using cluster surface models. J. Mol. Catal. A: Chem. 325 (1–2), 98–104.
Kuhn, M., Johnson, K., et al., 2013. Applied predictive modeling, Vol. 26. Springer.
Lietti, L., Nova, I., Camurri, S., Tronconi, E., Forzatti, P., 1997. Dynamics of the SCR-DeNO_x reaction by the transient-response method. AIChE J. 43 (10), 2559–2570.
Nova, I., Tronconi, E., 2014. Urea-SCR technology for de-NO_x after treatment of diesel exhausts, Vol. 5. Springer.
Nova, I., Ciardelli, C., Tronconi, E., Chatterjee, D., Bandl-Konrad, B., 2006. NH_3-SCR of NO over a V-based catalyst: Low-T redox kinetics with NH_3 inhibition. AIChE J. 52 (9), 3222–3233.
Ranea, V., Vicente, J., Mola, E., Arnal, P., Thomas, H., Gambaro, L., 2000. Adsorption of H_2O on the (001) plane of V_2O_5: chemisorption site identification. Surf. Sci. 463 (2), 115–124.
Senecal, P., Leach, F., 2019. Diversity in transportation: Why a mix of propulsion technologies is the way forward for the future fleet. Results in Engineering 4, 100060.
J. Teter, P. Cazzola, T. Gul, E. Mulholland, P. Le Feuvre, S. Bennett, P. Hugues, Z. Lagarde, V. Kraayvanger, T. Bryant, et al., 2017. The future of trucks: Implications for energy and the environment.
S. Gross, 2020. The challenge of decarbonizing heavy transport.
C. Sharp, G. Neely, B. Zavala, S. Rao, CARB low NO_x stage 3 program - final results and summary, Tech. rep., SAE Technical Paper (2021).
Song, I., Lee, J., Lee, G., Han, J.W., Kim, D.H., 2018. Chemisorption of NH_3 on monomeric vanadium oxide supported on anatase TiO_2: a combined DRIFT and DFT study. J. Phys. Chem. C 122 (29), 16674–16682.
Song, I., Lee, H., Jeon, S.W., Kim, T., Kim, D.H., 2020. Time-resolved observation of V_2O_5/TiO_2 in NH_3-SCR reveals the equivalence of Brønsted and Lewis acid sites. Chem. Commun. 56 (98), 15450–15453.
Suarez-Corredor, A.F., Babler, M.U., Olsson, L., Skoglundh, M., Westerberg, B., 2021. Characterization method for gas flow reactor experiments—NH_3 adsorption on vanadium-based SCR catalysts. Industrial & Engineering Chemistry Research 60 (30), 11399–11411.
Topsøe, N.-Y., 1994. Mechanism of the selective catalytic reduction of nitric oxide by ammonia elucidated by in situ on-line Fourier transform infrared spectroscopy. Science 265 (5176), 1217–1219.
Topsoe, N., Topsoe, H., Dumesic, J., 1995. Vanadia/titania catalysts for selective catalytic reduction (SCR) of nitric-oxide by ammonia: I. Combined temperature-programmed in-situ FTIR and on-line mass-spectroscopy studies, Journal of Catalysis 151 (1), 226–240.
Tronconi, E., Nova, I., Ciardelli, C., Chatterjee, D., Bandl-Konrad, B., Burkhardt, T., 2005. Modelling of an SCR catalytic converter for diesel exhaust after treatment: Dynamic effects at low temperature. Catal. Today 105 (3–4), 529–536.
Vittadini, A., Casarin, M., Selloni, A., 2005. First principles studies of vanadia- titania monolayer catalysts: Mechanisms of NO selective reduction. J. Phys. Chem. B 109 (5), 1652–1655.
Wachs, I.E., Weckhuysen, B.M., 1997. Structure and reactivity of surface vanadium oxide species on oxide supports. Applied Catalysis A: General 157 (1–2), 67–90.